The Impulsive Force of Debris Flow on a Curved Dam

Chjeng-Lun Shieh,[1)] Chia-Hsien Ting[2)] and Hung-Wen Pan[3)]
1) Deptartment of Hydraulic and Ocean Engineering, Cheng-Kung University, Tainan 70101, Taiwan (shieh@dprc.ncku.edu.tw)
2) Graduate School of Hydraulic and Ocean Engineering, Cheng-Kung University, Tainan 70101, Taiwan (n8891101@ccmail.ncku.edu.tw)
3) Graduate School of Hydraulic and Ocean Engineering, Cheng-Kung University, Tainan 70101, Taiwan (kevinpan@nckualumni.org.tw)

Abstract

Although sabo dams are efficient methods used in river and basin management, traditional sabo dams have a great impact on ecology and landscape. Moreover, such dams are hit and often damaged by great impulsive force when they block the flow of debris. Therefore, the forms of debris flow deserve thorough investigation. In this study, we designed a new form of sabo dam by changing the upstream-dam-surface geometric shape to reduce the impulsive force of the debris flow, with both enhanced stability and reduced need for concrete being the anticipated outcomes. In this study, the flume and laboratory facilities simulated the impulsive force of the debris flow to the sabo dams. Various geometric forms, including vertical-, slant- and curved-sabo dams, were used to determine the impulsive force. The results from both theory and experimental data clearly show that curved-sabo dams were hit by less force than other dams under the same debris flow. Impulsive force theories of the debris flow were derived from the moment equation and the Bernoulli equation. In these, the impulsive force was balanced by the friction force of the sabo dam and the opposite force of the load cell behind the dam as it was hit by the debris flow. Positive correlations were found when comparing the experimental data with the results computed from the theory. These findings suggest that our impulsive force theory demonstrates predictive validity with regard to the experimental data.

Keywords: debris flow, sabo dam, impulsive force, load cell

Introduction

It is important to construct sabo dams in rivers from viewpoint of basin management, as they can restrict the channel center line, reduce river bank erosion, and secure hillsides. As such, they are a common method of mountain management and flood disaster prevention. However, there are two great defects in traditional sabo dams: (1) with regard to ecology — cutting off migration routes; (2) with regard to landscape — using a large amount of concrete.

The purpose of this study is to solve the defects of traditional sabo dams by proposing a new form of curved-slit dam. (1) In the first experiment, we changed traditional trapezoid-dams to improved curved-dams in order to increase the length of dam-slope and thus reduce the debris flow force. The volume of the improved curved-dams could be decreased to use less concrete. (2) In the second experiment, we would change traditional closed-dams to curved-slit dams in order that water, undamaged sand and aquatic life could pass, thus avoiding ecological problems.

The curved-slit dam was first used in the management of a wild stream in Austria. The original concept was that the curved-slit dam could use less concrete and be impacted by less debris flow force, but there were few theories or experiment data that could predict or analyze the outcome. Curved breakwaters have also been widely employed in coast protection schemes.

The purpose of this study is to compare different forms of sabo dams by using theories and experiments: (1) Vertical dam (2) Slanted dam (3) Curved dam. Two load cells and one pressure gauge were used to measure dynamic pressure and static pressure of debris flow. A digital video camera was used to record the process of the experiments, and the motion of the impact of the debris flow could thus be shown. Estimating the impulsive force on a sabo dam is complex, because the force is influenced by various properties of the debris flow, particularly its mass, velocity and depth, as well as the properties of sabo dam itself, especially its shape.

At present, there have been few studies that discuss how debris flow is influenced by the shape of sabo dams. Takahisa Mizuyama (1979) separated the impulsive force of debris flow into fluid and boulder hit forces. The impulsive force on a vertical sabo dam has been described with fluid theories. Moreover, the theory

pp. 177–186

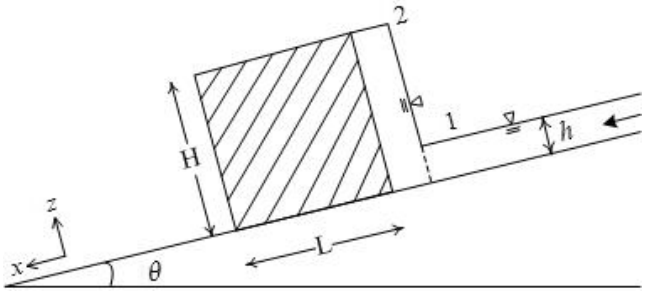

Fig. 1. Schematic diagram of impact process of debris flow on a vertical dam

of complete sphere elasticity was assumed so that the impulsive force of the boulders could be derived. Liu and Lee (1997) derived the control equation of debris flow from the continuity and momentum conservation equations. The effects of gravity, bottom stress, dynamic pressure, static pressure and shock pressure were all evaluated according to formula derived with experiment data. The total force calculated was very close to that measured experimentally. Lin and Huang (1999) experimented with the slope, angle and width of a slit dam. The tests investigated the trap efficiency, separation ability of particles and impulsive force of debris flow. The study showed that the trap efficiency and separation ability of particles were increased as the angle of the dam got larger, and the impulsive force on dams was decreased as the angle of the dam was reduced. Robert B. H. and Steven F. D. (2004) collided woody debris with structures using flume and test basin laboratory facilities. The tests investigated the maximum impulsive force that floodplain structures were exposed to from floating woody debris. Furthermore, the study used a single-degree-of-freedom model of collision. The laboratory data showed that the maximum impulsive force was associated with a log striking a rigid structure with its end.

Most of the studies have focused on determinations of impulsive force produced by debris flow, but few have considered the shape of the dam. Thus, this study was undertaken to examine the shape of dams with respect to impulsive force.

Method

Theory

According to The Second Law of Newton, the product of mass and acceleration is balance to force. $\overrightarrow{F}_{sys.}$ is the total force of a system, and the descriptive equation of $\overrightarrow{F}$ is

$$\sum \overrightarrow{F}_{sys.} = \frac{\partial}{\partial t} \iiint_{C.\forall.} \overrightarrow{V} \rho d\forall + \oint_{C.S.} \overrightarrow{V}(\rho \overrightarrow{V} \cdot d\overrightarrow{A}) \tag{1}$$

It is reasonable to assume that the debris flow is steady and the friction of the dam surface could be neglected. The Eq. (1) could thus be rewritten as

$$\sum \overrightarrow{F}_{sys.} = \oint_{C.S.} \overrightarrow{V}(\rho \overrightarrow{V} \cdot d\overrightarrow{A}) \tag{2}$$

The momentum variation of debris flow is influenced by the shape of dam. Thus, vertical, slanted and curved dams were used to derive the theories and experiments conducted in this study. When the dam is impacted by debris flow, the force on the dam is produced by the momentum variation of the debris flow. The impact processes of debris flow are shown in Figs. 1 to 3. The force herein is equal to the dynamic pressure of debris flow, and the equations of F_m are respectively

$$(F_m)_V = \rho_d V_1^2 h_1 b \tag{3}$$

$$(F_m)_S = \rho_d V_1^2 h_1 b - \rho_d V_2^2 b \cos\alpha \tag{4}$$

$$(F_m)_C = \rho_d V_1^2 h_1 b - \rho_d V_2^2 b \cos\beta \tag{5}$$

where F_m = force produced by momentum change; ρ_d = density of debris flow; V_1 == velocity of the debris flow front close to the dam; V_2 = velocity of the debris flow front on the dam; h_1 = depth of the debris flow front close to the dam; h_2 = depth of the debris flow front on the dam; b = width of the dam; α = angle of the slanted dam; β included angle of debris flow front and input position.

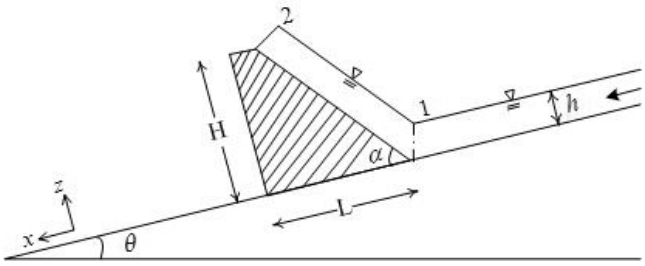

Fig. 2. Schematic diagram of impact process of debris flow on a slanted dam

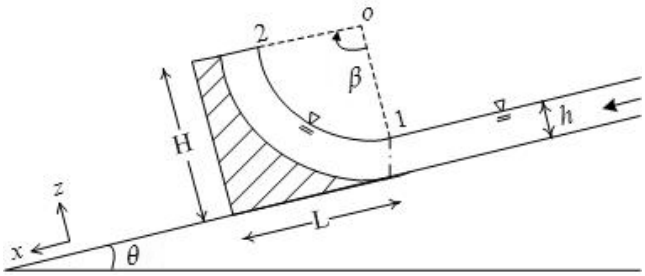

Fig. 3. Schematic diagram of impact process of debris flow on a curved dam

When the debris flow front flowed through the dam surface, the depths were not the same ($h_1 \neq h_2$). The Bernoulli equation could be written as

$$\frac{P_1}{\gamma} + \frac{V_1^2}{2g\cos\theta} + Z_1 = \frac{P_2}{\gamma} + \frac{V_2^2}{2g\cos\theta} + Z_2 \tag{6}$$

Since, $P_1 = P_2 = 0$ Eq. (6) becomes

$$V_1 = [V_1^2 - 2g\cos\theta(Z_2 - Z_1)]^{1/2} \tag{7}$$

Considering the integral continuity equation

$$\frac{\partial}{\partial t}\iiint_{C.\forall} \rho_d d\forall + \oint_{C.S.} \rho_d \overrightarrow{V} \cdot d\overrightarrow{A} = 0 \tag{8}$$

Assuming that debris flow was steady, and Eq. (8) is simplified as

$$\oint_{C.S.} \rho_d \overrightarrow{V} \cdot d\overrightarrow{A} = 0$$

or

$$h_1 V_1 = h_2 V_2 \tag{9}$$

Substituting Eq. (7) into Eq. (9),

$$h_2 = \frac{V_1 h_1}{[V_1^2 - 2g\cos\theta(Z_2 - Z_1)]^{1/2}} \tag{10}$$

Substituting Eq. (7) and Eq. (10) into Eq. (3), Eq (4) and Eq (5),

$$(F_m)_V = \rho_d V_1^2 h_1 b \tag{11}$$

$$(F_m)_S = \rho_d V_1^2 h_1 b - \rho_d V_1 h_1 b[V_1^2 - 2g\cos\theta(z_2 - z_1)]^{1/2}\cos\alpha \tag{12}$$

$$(F_m)_C = \rho_d V_1^2 h_1 b - \rho_d V_1 h_1 b[V_1^2 - 2g\cos\theta(z_2 - z_1)]^{1/2}\cos\beta \tag{13}$$

Eq. (11), Eq (12) and Eq (13) are average forces produced by dynamic pressures of debris flow from point 1 to point 2 in Figs. 1 to 3.

Experiments

The flume used in this study was 0.2 m wide × 0.5 m high × 8 m long. It allowed tests with the water and material moving and the sabo dam remaining stationary. Three kinds of sabo dam were used to measure the impulsive force on stationary load frames placed above and behind the dam. Two load frames had rectangular targets mounted on two fixed ends, which in turn were mounted on two load cells that were fastened to rigid frames mounted on the flume. In the flume tests we varied the shapes of the sabo dams, discharges and slopes of flume. The three shapes of the dams were vertical, slanted and curved. The upstream tank was stored with 0.1 m, 0.2 m, and 0.3 m depth of water for three different discharges. The flume slopes of 6° and 10° were used in the tests. To simplify tests, gravel with an average diameter of 3.6 mm was used. The schematic diagrams of the flumes are shown in Figs. 4 and 5. The load cells and pressure gauge set are shown in Figure 6.

The sabo dams were composed of acrylic planks. The thickness of each acrylic plank was 8mm. The schematic diagrams of the three dams are shown in Figs. 7 and 8. In decreasing order, the volumes of the dams were vertical, slanted and curved. The lengths of the flow paths on the dams were curved, slanted and vertical. In tests, an experimental serial number was used for the "dam shape-slope-discharge", such as "V-6-10".

Results

The momentum variations of debris flow through dams were different due to the different shapes. The relations $z_2 - F_m$ associated with "V, S, C-6-30" and "V, S, C-10-30" were computed by Eq. (11) to Eq. (13) as shown in Figure 9. The diagram shows that the momentum variation of debris flow in the vertical dam was larger than other dams, because of its vertical surface. In the slanted and curved dams, dynamic pressure of debris flow was dispersed due to their slanted or curved surfaces. Moreover, the line of the curved dam was raised much more smoothly than that of the slanted dam. At $z_2 \cong 0.15m$ (half of the dam height), the dynamic pressure of the slanted dam was the same as the one of the curved dam; at $z_2 < 0.15m$, the values of the slanted dam were larger than those of curved dam; at $z_2 > 0.15m$, the values of slanted dam were smaller than those of curved dam.

Figs. 10, 11 and 12 shows the tests results for "V-6-30", "S-6-30" and "C-6-30". The diagram indicates that the sabo dam produces large forces immediately when debris flow contacts with it. This is because the energy of debris flow was dispersed when the flow was blocked by the sabo dams. At the beginning of the impact, the dynamic pressures were the main force produced by debris flow; then, the dynamic pressures and static pressures existed simultaneously, as the debris flow in front of the dams became strongly turbulent. After the debris flow stopped, the static pressures were the main force produced as debris was deposited in front of the dams and the depth of water increased.

The descriptive equations of impulsive force could be obtained by the force balance condition, as follows

$$\begin{aligned}(F_1)_{V,S,C} + [(F_b)_{V,S,C}\cos\theta - (F_L)_{V,S,C} + (F_d)_{V,S,C}\cos\theta]\mu_s - (F_b)_{V,S,C}\sin\theta \\ = (F_m)_{V,S,C} + (F_d)_{V,S,C}\sin\theta \end{aligned} \quad (14)$$

Where F_1 = the value of the load cell in the x direction; F_b = body force; F_L = buoyancy; F_m = dynamic pressure; F_d = static pressure. The left of the equal sign is the measured impulsive force $\bar{F}_M$, and the right of the equal sign is the theoretical impulsive force $\bar{F}_T$. Eq. (14) then becomes

$$\bar{F}_M = (F_1)_{V,S,C} + [(F_b)_{V,S,C}\cos\theta - (F_L)_{V,S,C} + (F_d)_{V,S,C}\cos\theta]\mu_s(F_b)_{V,S,C}\sin\theta \quad (15)$$

$$\bar{F}_T = (F_m)_{V,S,C} + (F_d)_{V,S,C}\sin\theta \quad (16)$$

In the x direction, the impulsive force of debris flow is balanced by the friction force and load cell. Thus, the impulsive force is equal to the sum of values of the load cell and friction force subtracted from a component of body force along the flume. Comparing $\bar{F}_M$ with $\bar{F}_T$, we can find out the positive correlation with the measured and theoretical data for different experiment conditions, as shown in Fig. 13. This shows that the theories could well describe the experiment results. As Fig. 14 indicates, the maximum forces measured on the slanted dam were smaller than those of the vertical dam in general. This is because the slanted surface could disperse a part of the force, while the vertical surface took all of the force. As Fig. 15 shows, the maximum forces measured on the curved dam were smaller than those of the vertical dam in general. Although the variations of momentum produced by debris flow on the curved dam and vertical dam were the same, the maximum force measured on the curved dam was small due to its curvature and long path. The curvature let variations of momentum be different along the dam surface. The long path let the impact time increase and the force decrease. Ratios of $\bar{F}_M/F_{Max.}$ against F_r are shown in Fig. 16. As the diagram indicates, the ratios

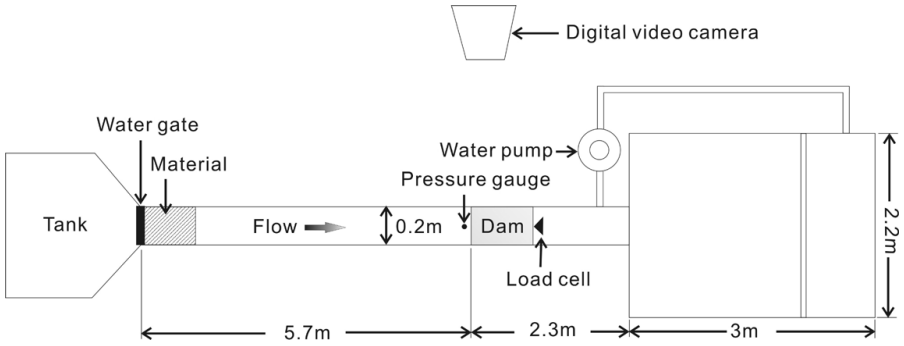

Fig. 4. Schematic diagram of the flume (A vertical view)

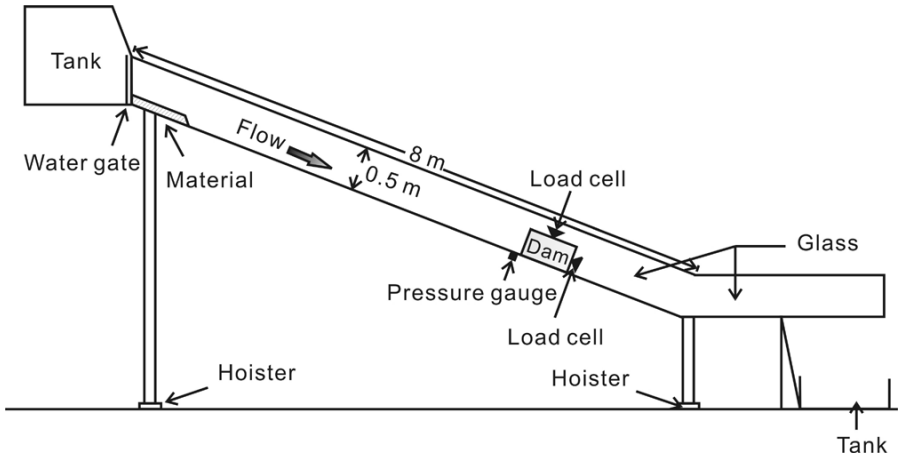

Fig. 5. Schematic diagram of the flume (A lateral view)

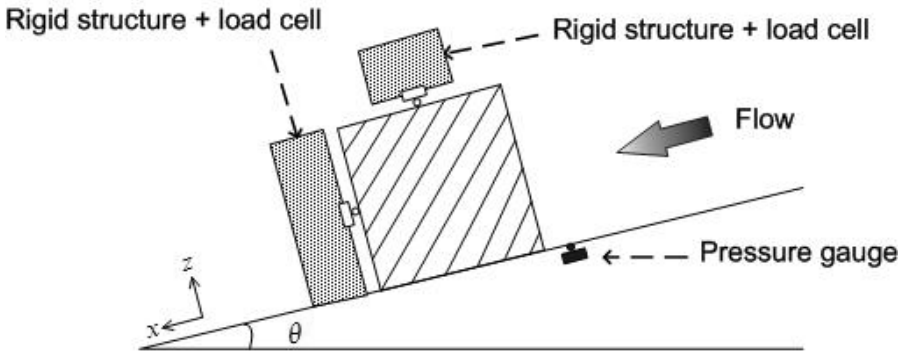

Fig. 6. Schematic diagram of the measurement system

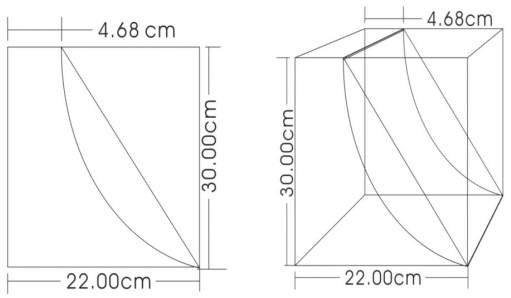

Fig. 7. Schematic diagram of three dams

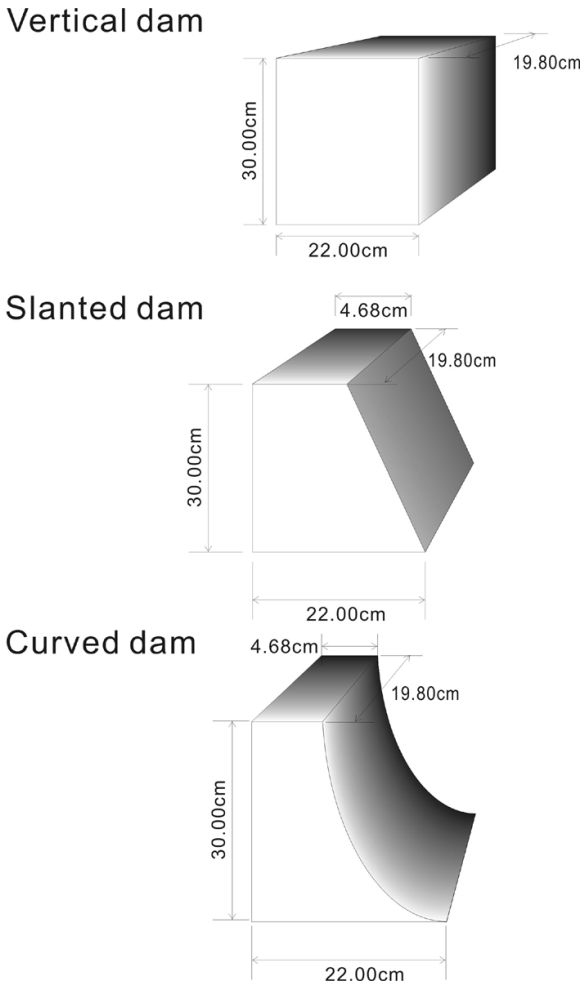

Fig. 8. Schematic diagram of three dams

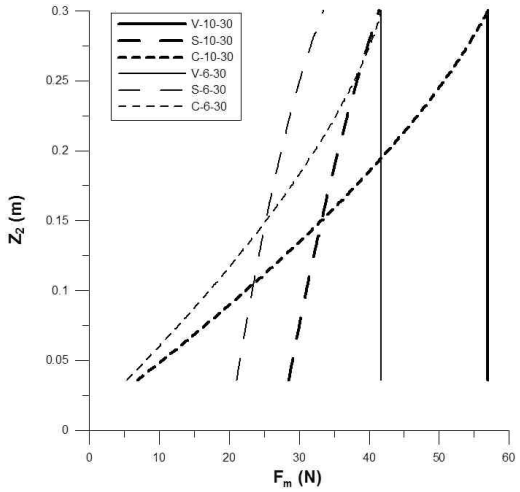

Fig. 9. Relational diagram of $z_2 - F_m$ in "V-6-30" and "V-10-30"

rise as F_r increases. Thus, $\bar{F}_T$ was close to $F_{Max.}$ when F_r was increasing. The result showed that dynamic pressures of debris flow are the main force on sabo dams, especially on curved dams.

The shapes of deposits of debris flow were different due to the different shapes of the dams. Figs. 17, 18 and 19 show the shapes of deposits on the three dams. The depth of the deposits rises as discharges increase.

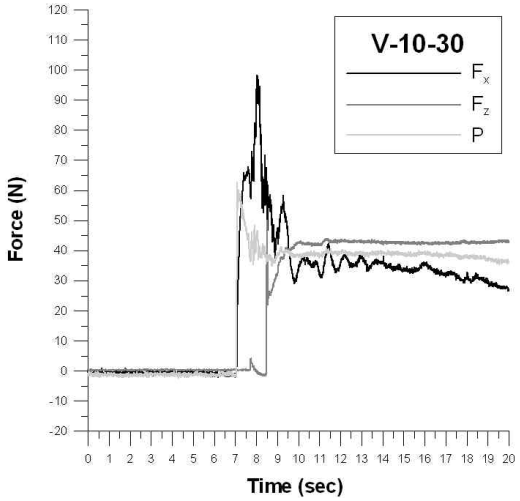

Fig. 10. Variational diagram of force and time for "V-10-30"

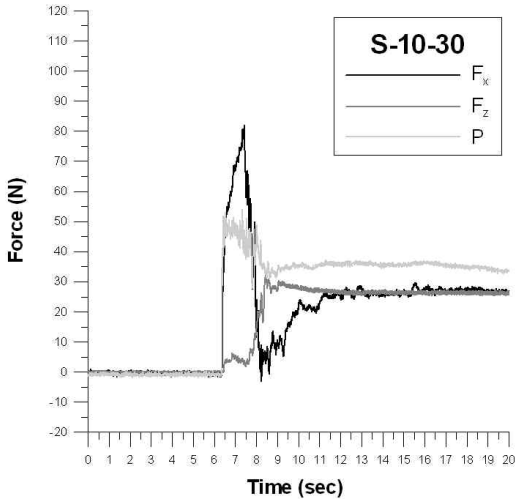

Fig. 11. Variational diagram of force and time for "S-10-30"

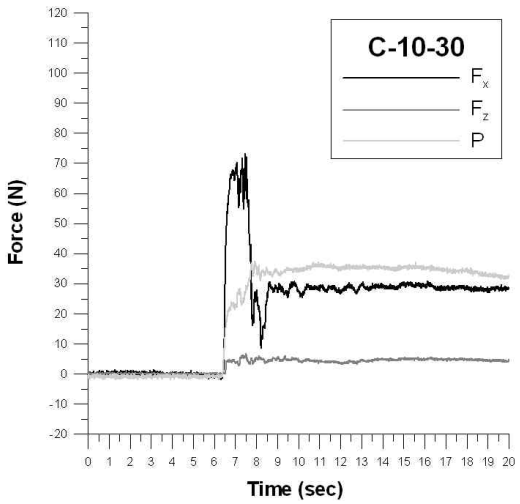

Fig. 12. Variational diagram of force and time for "C-10-30"

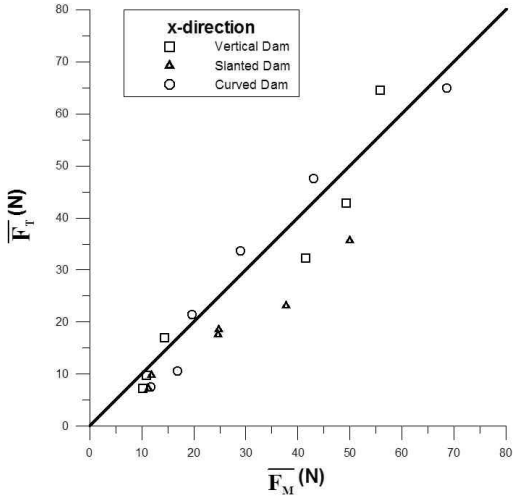

Fig. 13. Relational diagram of the measured and theoretical impulsive force

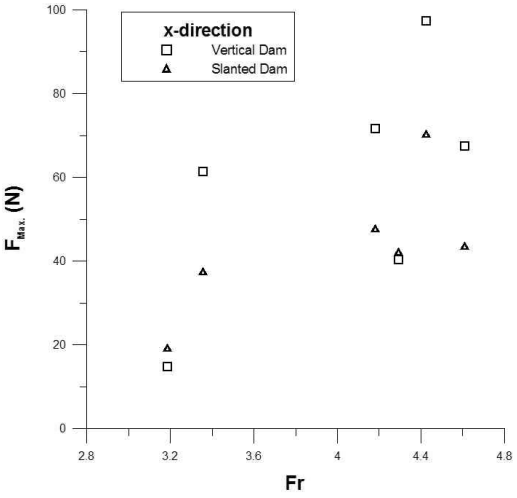

Fig. 14. Relational diagram of maximum force with vertical dam and slanted dam

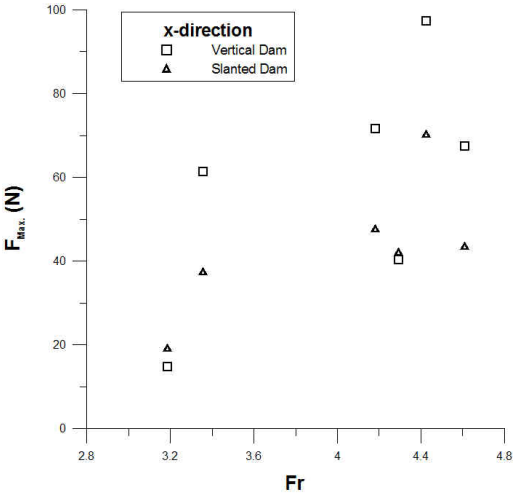

Fig. 15. Relational diagram of maximum force with vertical dam and curved dam

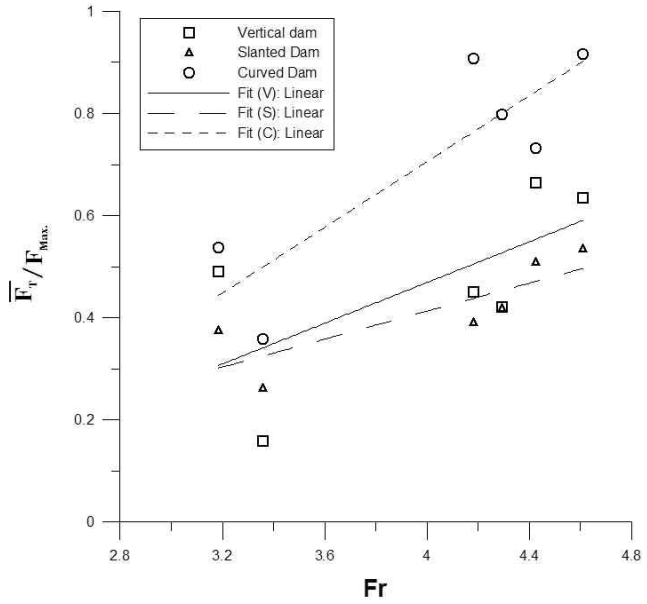

Fig. 16. Relational diagram of on three dams

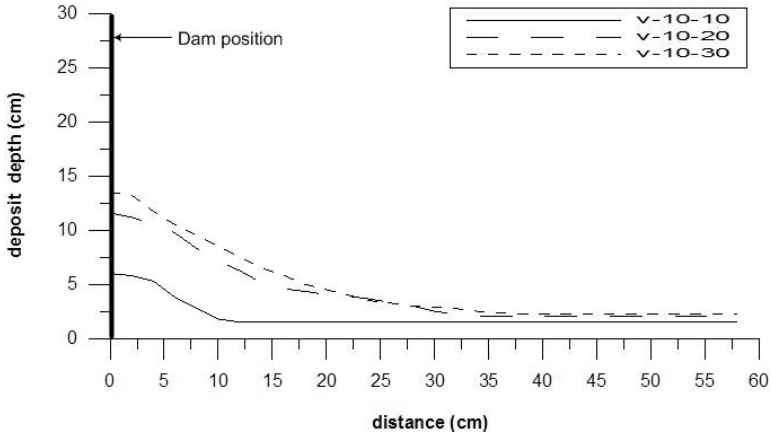

Fig. 17. Diagram of deposits for the vertical dam

Since most of deposits were caught in front of the vertical dam, the trap efficiency of the vertical dam was higher than those of other dams; debris flow would flow along the slanted surface to the downstream area. Although some materials would be deposited in front of the slanted dam, some would be taken to the downstream area. Thus, the trap efficiency of the slanted dam was lower than those of other dams; debris flow would flow along the curved surface to the downstream and upstream areas, and the latter reduced the energy of the following debris flow. The shape of deposits on the curved dam could lead to large friction and restoring moment. As a result, the stability of the curved dam was better than the others.

Conclusions

From what has been discussed above, we can conclude that curved-sabo dams are impacted by less force than other dams under debris flow. Moreover, the stability of curved-sabo dams is better than with other dams. Enhanced stability and less need for concrete are thus anticipated. Based on the laboratory data, we find that the impact geometry has a significant effect on the impulsive force. The time duration of the impact on the dam is long, and the force impacted on the dam is less. Furthermore, estimating the impulsive force on the dam is complex because the force is influenced by the properties of the debris flow, particularly its mass and velocity. In this study, we use the average velocity of debris flow to estimate the impulsive force. If we can measure the velocity more accurately in the experiment, our results will improve.

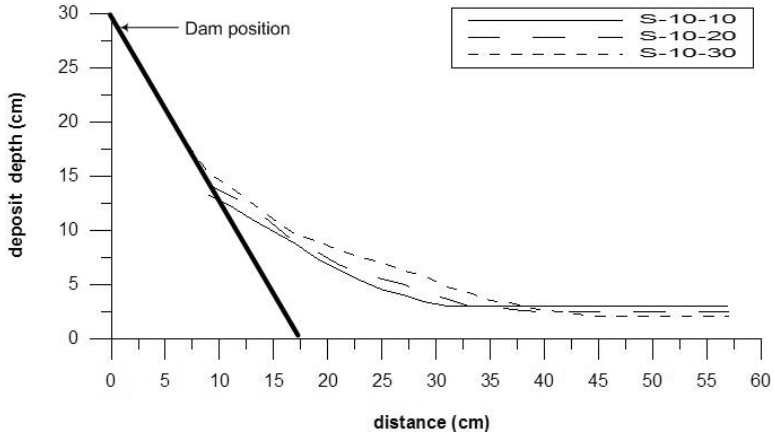

Fig. 18. Diagram of deposits for the slanted dam.

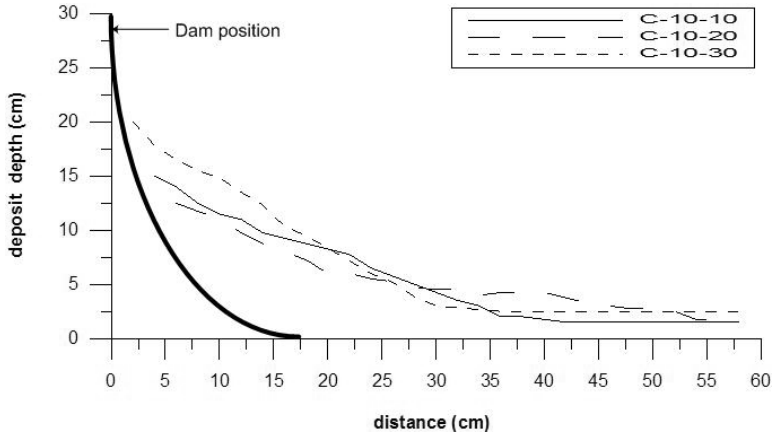

Fig. 19. Diagram of deposits for the curved dam.

References

Haehnel, R.B. and Daly S.F. (2004) *Maximum Impulsive force of Woody Debris on Floodplain Structures*, Journal of Hydraulic Engineering, p.112–120.

Lin, P.S. and Huang, Y.C. (1999) *A study of the effect in concrete slit sabo dam*, Master Paper of National Chung Hsing University, Taiwan.

Liu, K.F. and Lee, F.C. and Tsai, H.P. (1997) *Flow field and impulsive force on a debris dam*, International Conference on Debris-Flow Hazards Mitigation: Mechanics, Prediction, and Assessment, Proceedings, ASCE, 1997, p.737–746.

Takahisa M. (1979) *Computational Method and Some Considerations on Impulsive Force of Debris Flow Acting on Sabo Dams*, J. of the Japan Society of Erosion Control Engineering, 112, p. 40–43.